

PAPER

Ground and geostationary orbital qualification of a sunlight-stimulated substrate based on shape memory polymer composite

To cite this article: Fengfeng Li *et al* 2019 *Smart Mater. Struct.* **28** 075023

View the [article online](#) for updates and enhancements.

Ground and geostationary orbital qualification of a sunlight-stimulated substrate based on shape memory polymer composite

Fengfeng Li¹, Liwu Liu¹, Xin Lan¹, Chengtong Pan¹, Yanju Liu¹ , Jinsong Leng¹  and Qiong Xie²

¹Harbin Institute of Technology, 150001 Harbin, People's Republic of China

²Institute of Telecommunication Satellite, CAST, 100094 Beijing, People's Republic of China

E-mail: lengjs@hit.edu.cn

Received 9 January 2019, revised 31 March 2019

Accepted for publication 12 April 2019

Published 6 June 2019



CrossMark

Abstract

A sunlight-stimulated substrate, named Mission SMS-I, carried out the orbital deployment experiment and anti-irradiation verification on an experimental geostationary satellite. It is the prototype of a solar array substrate which integrates the conventional substrate, support structure, and deployment function by using the carbon fabric reinforced shape memory polymer composite (SMPC). The substrate could deploy from the 'Ω' packaged configuration to the '∩' deployed configuration once its temperature is at or above the glass transition temperature. This paper presents details of the Mission SMS-I in a sequence of material preparation, structure design, manufacture, ground experiments, and orbital experiment. Results show that the Mission SMS-I can withstand the required mechanical and thermal conditions, successfully deploy in orbit and have a good long-term anti-irradiation capability. SMPC is a suitable choice for the substrate of solar arrays or any other deployable structures which need the actuation in material-level or directly exposed to the space environment.

Supplementary material for this article is available [online](#)

Keywords: shape memory polymer composite, geostationary orbital experiment, sunlight-stimulated, shape recovery

(Some figures may appear in colour only in the online journal)

1. Introduction

The solar array is often the source of the spacecraft primary and reliable electrical power to run the sensors, telemetry, propulsion, etc [1–3]. It is usually folded during spacecraft launch and unfolded at operational stage. In that way, most solar arrays fall into the category of deployable structures. It could be briefly divided into rigid and flexible arrays. Common rigid arrays get their name for honeycomb sandwich panels which are arranged in series/parallel and connected by hinges [4–8]. The solar cells which are mounted onto the rigid panels normally are thin crystal silicon and multi-junction

gallium arsenide (GaAs) based photovoltaic cells [9]. The rigid solar arrays are suitable for low to mid power supplement [10]. Nowadays, with the need for deep space exploration, high power and efficient solar arrays are essentials for the spacecraft design. The advancement in photovoltaic cell efficiency over the past years has made up with some of the power demand, but still not in excess of the spacecraft power demand. Thus, at the spacecraft level, more panels, hinges and support structures are added, which lead to the complexity of deployment kinematics [10–13]. Their support frameworks, deployment mechanisms, and these associated launch controls and restrictions, sometimes

account for $\sim 90\%$ of the weight budget of the deployment assembly [14, 15]. Consequently, flexible solar arrays with the advantages of low mass, low cost, and high specific power come into people horizon. The first operational flexible solar array is believed on Canadian Technology satellite, Hermes, which was flown on January 1976 [16]. Today's well-known flexible solar arrays are on the International Space Station (ISS). Both of them are composed of blankets, which are folded up to accordion-fashion during launch or ascent and unfolded by deployable mast or truss. Unlike the accordion folding method, roll out solar array (ROSA), which consists of rollable photovoltaic cells, tensioned-membrane blanket array and deployable tubular booms, is more like a tape measure. It is rolled up in the storage stage and unreels along with the tubular booms deployment [10]. It was deployed and then jettisoned from the ISS on July 2017. Various flexible solar arrays have been developed, but few of them have flown in earth orbits. Even though, researchers still put efforts into the development of new solar arrays. To get high stowed packing efficiency and low mass level, new solar cells, substrates, and support structures may be needed in conjunction with the new deployment method.

Shape memory polymer (SMP) can transform from a temporary deformed shape to the original shape under certain stimuli [17–20]. Since the discovery of SMP, research efforts are on material fabrication, shape memory mechanism and application exploration [17–23]. The low stiffness of pure SMP makes it unusable for high-load working conditions. Thus the fiber reinforced shape memory polymer composite (SMPC) emerges with its advantages of low density and cost, high stiffness and strength, and high damping capability, etc [24–28]. For heat-induced SMP/SMPC, the shape memory cycle starts from the original undeformed shape, then the temperature of the material is reached above its glass transition temperature (T_g), followed by the deformation SMP/SMPC by the external force. Next, the SMP/SMPC is cooled below the T_g with constraint. Once the temporary shape is fixed, the external constraint is removed. When reheating the material above T_g , it recovers to its original shape [17–20]. Shape memory property, the most distinguished property of SMP/SMPC, has made the material a promising choice for deployable structures since the structures can be packaged and deployed without complex mechanical devices [29–35]. There would be a variety of applications of SMPC on spacecraft, such as trusses, radiators, and solar arrays [29–35]. SMP/SMPC can also be combined with origami technology, considering the pattern and behavior of origami are suitable for designing large deployable structures. The Composite Technology Development Inc., Lafayette, CO (CTD) has been working for many years to develop the TEMBO[®] Elastic Memory Composite, referred to as EMC. Some of their products have been carried out the spaceflight experiments, including the EMC hinge which consists of two arch-shaped EMC laminates connected by two end connectors, and the FalconSAT-3 deployable gravity gradient boom which is designed with central sleeves and EMC laminates longerons [30, 34, 35]. Recently, researchers from Italy has been joined the SMP/SMPC spaceflight experiments in material-level. In

2011 and 2013, I-FOAM (three SMP foam samples under compression, bending and torsion loading), and RIBES/FOAM2 (three samples of a compressed SMP foam, a SMP foam actuator and a SMPC sheet), have been conducted in succession to test their shape recovery property in micro-gravity conditions [36, 37]. Those published spaceflight experiments of SMP/SMPC are all conducted in low earth orbit. In order to expand the applications of SMP/SMPC on spacecraft, the proto-flight experiments in geostationary orbit need to be done.

In 2016, Mission SMS-I, a prototype for solar array substrate based on carbon fabric reinforced SMPC, has been carried out on an experimental satellite to geostationary earth orbit. It is mounted on the satellite deck, directly exposed to the space environment. The goals of this mission could be categorized into two; the first is to test the shape recovery behavior of the substrate actuated by sunlight, the second is to verify the anti-irradiation capacity after long-term space exposure. The details of material fabrication and mechanical experiments at different temperatures are presented in section 2, followed by the structure geometry design and finite element method (FEM) simulation, structure assembly in section 3. Section 4 presents a series of ground experiments, including vibration, shock, vacuum thermal cycling, and ground-based deployment experiments, which are conducted to ensure the structure could endure launch and space environments. The orbital verification is presented in section 5. A conclusion is drawn in section 6, followed by the perspectives in section 7.

2. Preparation of material

2.1. Material fabrication

The matrix of the composite used in this project belongs to the epoxy based SMP series developed by Jinsong Leng's group [38]. It has completed ground simulated space environment tests (plasma environment, atomic oxygen, ultraviolet radiation and vacuum thermal cycling), demonstrating its suitability for aerospace applications [39, 40]. The reinforcement was plain weave carbon fabric CO6343B, TORAY. The manufacture method was vacuum assisted resin infusion.

Because the Mission SMS-I is in geostationary orbit, charged particles would accumulate on the surface of the substrate and need to be dissipated to avoid breakdown. For meeting the requirement of relatively high stiffness and good electrical conductivity, the composite was developed with four layers: three fabric layers in fiber orientation of $-45^\circ/45^\circ$, and a layer of chopped carbon fiber at the top. The chopped carbon fiber was cut from the CO6343B used in this study, ranging in length from 6 to 8 mm due to the manufacturing deviation. It is weight fraction is $\sim 0.58\%$. The curing was performed in a programmable temperature oven with the process of 80°C for 3 h, 100°C for 3 h and 150°C for 5 h. After demoulding, the composite was polished at the chopped carbon fiber surface to expose the fiber to the air.

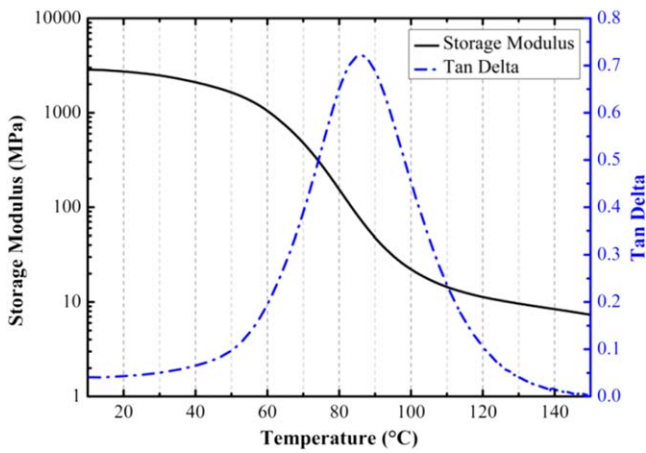


Figure 1. Results of dynamic mechanical analysis of SMP.

The polishing was stopped till the resistance between any two points on the surface was basically between 100 and 1000 Ω . The final thickness of the composite was about 0.84 mm.

2.2. Material experiments

A dynamic mechanical analysis (DMA) test was conducted on a DMA 242 C analyzer (NETZSCH Instruments, Germany) with the tensile mode over a frequency of 1 Hz. The temperature increased from 10 °C to 150 °C at a constant heating rate of 3 °C min⁻¹. The dimension of the specimen was 19.00 mm × 3.00 mm × 0.72 mm. Results are presented in figure 1. The transition range starts from ~60 °C and nearly stops at ~110 °C. The temperature corresponding to the peak of the tan delta is defined as T_g which is 85.4 °C, ensuring the SMP could be stimulated by sunlight. The storage modulus at low temperature (<40 °C) is above 2.0 GPa, while below 11.0 MPa at high temperature (> 120 °C).

Isothermal three-point bending experiment according to the ASTM D790-17 standard was carried out for two kinds of SMPC specimens: Series A and Series B. They had the same dimension 60.00 mm × 12.07 mm × 0.84 mm. Series A was original, which has never been deformed. Series B has been curved with a radius of 10 mm and then deployed to the flat configuration. This was arranged to verify the deformation influence on materials' mechanical properties. All experiments were conducted on Zwick Z010 universal testing instrument (Zwick GmbH, Ulm, Germany) equipped with a temperature chamber. The targeted temperatures were 25 °C, 50 °C, 75 °C, 100 °C, and 125 °C. The support span was 25.4 mm. The test terminated when the strain of the outer surface reached 5%. At least five specimens were tested for each condition.

Figure 2 demonstrates both Series A and B show temperature dependent mechanical properties. Their moduli decrease with the increase of temperature, an obvious turning point is observed at 75 °C since it closes to T_g of 85.4 °C. Moduli for two series at 25 °C are 5.26 GPa, 4.99 GPa respectively, one order of magnitude higher than those at 125 °C (0.37 GPa for Series A, 0.23 GPa for Series B). Series B has lower flexural modulus and strength, the reduction rates

of modulus compared to Series A are 5.2% (25 °C), 17.8% (50 °C), 29.2% (75 °C), 45.8% (100 °C), and 33.2% (125 °C); while 7.3% (25 °C), 17.6% (50 °C), 30.5% (75 °C), 45.5% (100 °C), and 41.8% (125 °C) for the reduction rates of flexural strength. This is due to the micro-buckling of the fabric, which allows the composite survive under large bending deformation, but it might cause unavoidable internal damage. Nevertheless, the mechanical properties of the deformed SMPC are still higher than the SMP. Here we have to mention that the SMPC is mainly a functional material in most applications, and its deformability and shape memory property are our primary consideration. Since there is no reduction of both properties, the deformed SMPC is still acceptable.

3. Structure design and assembly

3.1. Geometry design

The design of SMPC-based sunlight-stimulated substrates have drawn on the accordion-fashion folding method of the conventional hinged-panel solar arrays, but are integrally formed where all hinges span the entire width of the panel. And the hinges are made directly by the same material of the panel, which is the carbon fiber reinforced SMPC in this study. It is packaged from the original flat configuration to the accordion-fashion before launch. When the deployment operation is required in orbit, the spacecraft can be commanded to adjust its attitude to expose the SMPC-based substrate to the Sun, stimulating the substrate to deploy to the flat configuration. Either rigid or rollable photovoltaic cells could be mounted on it, since it has large undeformed areas (vertical lines in figure 3(a)) for any type of solar cells. It is a reasonable alternative for the solar arrays in CubeSats or SmallSats with merits of light weight, small volume, relatively high stiffness and power-saving since it can deploy without the satellite energy supply.

Mission SMS-I is a prototype of the future sunlight-stimulated substrate. The substrate is developed with one unit, exhibiting 'Ω' packaged configuration, while '-' deployed configuration. The prototype consists of a substrate, base, cap, screws, thermistor, and multi-layer insulation (figure 4). The substrate is placed between base and cap, and fixed by four screws at the corner. The base is designed like a chair with four feet attached to a flat plate, it is used to support the substrate and connect the whole structure to satellite. The thermistor is arranged to collect temperature data in orbit, placed inside the base and stuck to the other surface of base under the substrate. The Multi-layer insulation is covered around the base mainly to isolate the heat flow. The design criteria are:

- Total weight should be less than 0.5 kg;
- Envelope size should be within the following:
133 mm (length) × 100 mm (width) × 120 mm (height) in packaged configuration,

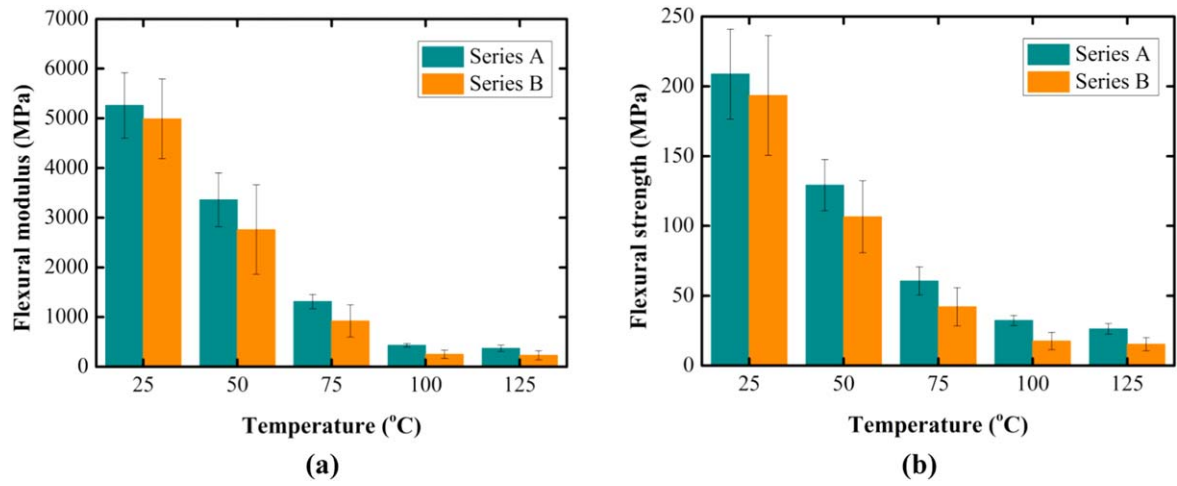


Figure 2. Three-point bending test results of SMPC at different temperatures, (a) flexural modulus, (b) flexural strength.

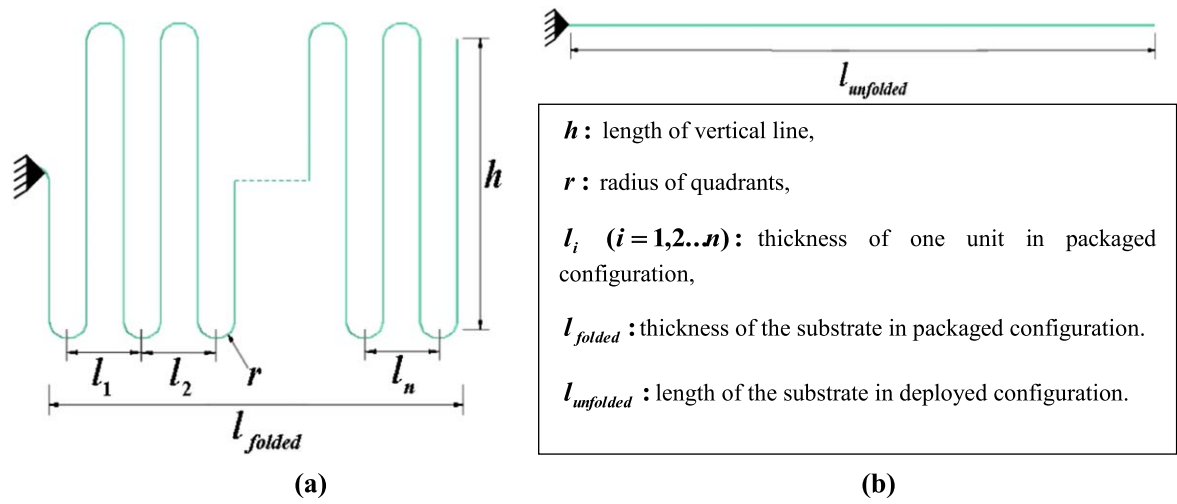


Figure 3. Schematics of the future sunlight-stimulated substrate in packaged and deployed configurations, (a). Packaged configuration, (b). Deployed configuration.

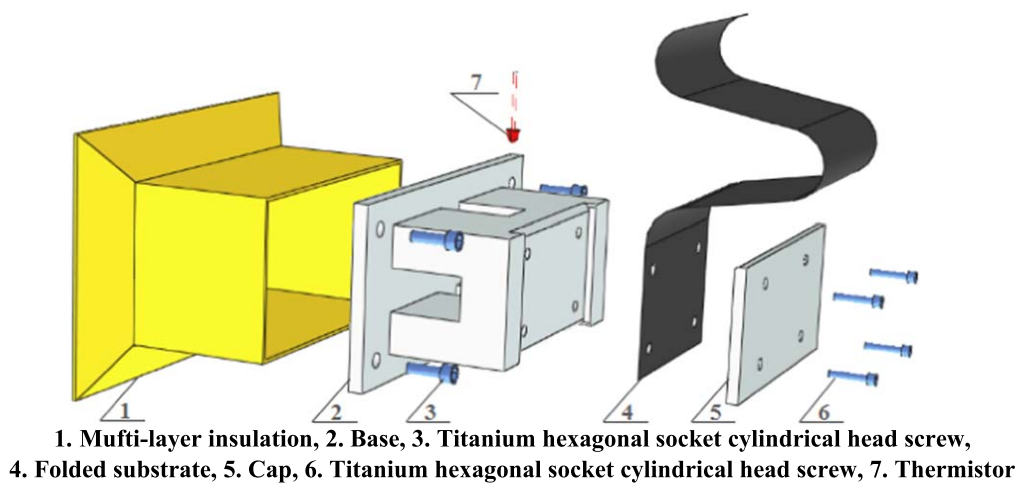


Figure 4. Components of Mission SMS-I.

Table 1. Parameters of the substrate in the parametric study.

No. of condition	r mm	h mm	w mm	l_{folded} mm	$l_{unfolded}$ mm
1	10	30	50	50	138.5
2	10	30	40	50	138.5
3	10	30	60	50	138.5
4	10	40	50	50	158.5
5	10	20	50	50	118.5
6	13	30	50	65	162.05
7	16	30	50	75	177.75

Table 2. Ply method of the carbon fiber reinforced epoxy-based SMPC.

No. of layer	Thickness (mm)	Orientation angle (°)
1	0.14	45
2	0.14	-45
3	0.14	45
4	0.14	-45
5	0.14	45
6	0.14	-45

230 mm (length) \times 100 mm (width) \times 61 mm (height) in deployed configuration;

- c. The recovery ratio of the Sunlight-stimulated substrate should not be less than 95%;
- d. The first order of natural frequency should be higher than:
 - 30 Hz in the packaged configuration,
 - 2 Hz in the deployed configuration;
- e. The structure should withstand required mechanical and thermal experiments, including sine vibration,

random vibration, shock experiment, and vacuum thermal cycling experiment.

Geometry parameters of the substrate (width w , radius r and length h) are critical to the unfolding/folding ratio and natural frequency of the structure. According to the above criteria, parametric study has been done by the FEM, here we select seven conditions (table 1) to show the general impact of the parameters on the natural frequency of the structure. Results will be shown in the next section. Due to the bending properties of the SMPC used in this study, the minimum radius is 10 mm.

3.2. Simulation

Abaqus simulation is used to aid the design. The finite element model was simplified into three parts: the Sunlight-stimulated substrate, base, and cap. The substrate was established by shell part, while the others were solid parts. The connections among interfaces were tie constraint. The surfaces of screw holes at the bottom of base were fixed in all directions as boundary conditions.

The base and cap were made of aluminum alloy: elastic modulus 70 GPa, Poisson's ratio 0.33, and density 2700 kg m⁻³. The material of substrate was simplified as a symmetric cross-ply laminate, which was composed of six layers, every layer has its specific orientation and thickness, as shown in table 2. The basic mechanical parameters of each layer are shown in table 3, the parameters at 25 °C were used in packaged configuration, while those at 100 °C were used in deployed configuration since the substrate softened when irradiated by sunlight in orbit. The chopped carbon fiber layer was ignored since its reinforcement was not obvious. The density of SMPC is 1500 kg m⁻³.

The Mission SMS-I substrate in packaged configuration is like a cantilever spring. The vibration modes of the seven

conditions are similar, here we take the condition 1 for demonstration (figure 5). The first order vibration mode shows an outward swing along the axis X . The second mode is a rear-end squat mainly caused by the curved middle part. The third is a rotation along axis X , and the fourth is a torsion along axis Z . Table 4 lists the first four orders of natural frequencies of the above seven conditions. Conditions 1–3 show that the width of the substrate has little impact on the first three natural frequencies, but the fourth increases with the width decrease. Conditions 1, 4 and 5 reveal that the smaller height h leads to higher the natural frequency. Though large height results in a higher unfolding/folding ratio, we still eliminate the condition 4 since its first natural frequency is below 30 Hz. Conditions 1, 6 and 7 indicate that the smaller the bending radius, the higher the structure's stiffness.

The sunlight-stimulated substrate stretches like a cantilever in its deployed configuration. The mode shapes of the seven conditions are similar to the cantilever (figure 6), which are: bending along axis Y (the 1st order), torsion along axis X (the 2nd order), wave in longitudinal (the 3rd order), and torsional combination in opposite directions along the axis X (the 4th order). The natural frequencies are listed in table 5. Conditions 1–3 indicate that the natural frequency of the structure increases with the w increase. Conditions 1, 4–8 show that the increase in length reduces the stiffness of the substrate. Only conditions 1, 3, and 5 meet the first order of natural frequency requirement in the criteria. Condition 1 stands out for its light weight compared to condition 3 and high unfolding/folding ratio compared to the condition 5. The final w , r , and h are 50 mm, 10 mm, and 30 mm respectively.

3.3. Structure assembly

Figure 7 demonstrates the manufacturing process of the Sunlight-stimulated substrate. Material fabrication has been introduced in section 2.1. After material fabrication, the SMPC laminate was cut into rectangles with 50 mm width and 180 mm length by CNC engraving and milling machine. Then, heat the SMPC substrate in a vacuum drying oven to \sim 100 °C, along with the deformation mold which consisted of the male die and female die. After soaking at high temperature for 20 min, the soften SMPC substrate was gently punched to female die by male die outside the oven. This whole set was put into the oven again with the external load placed at the top. The process of reheating was to release

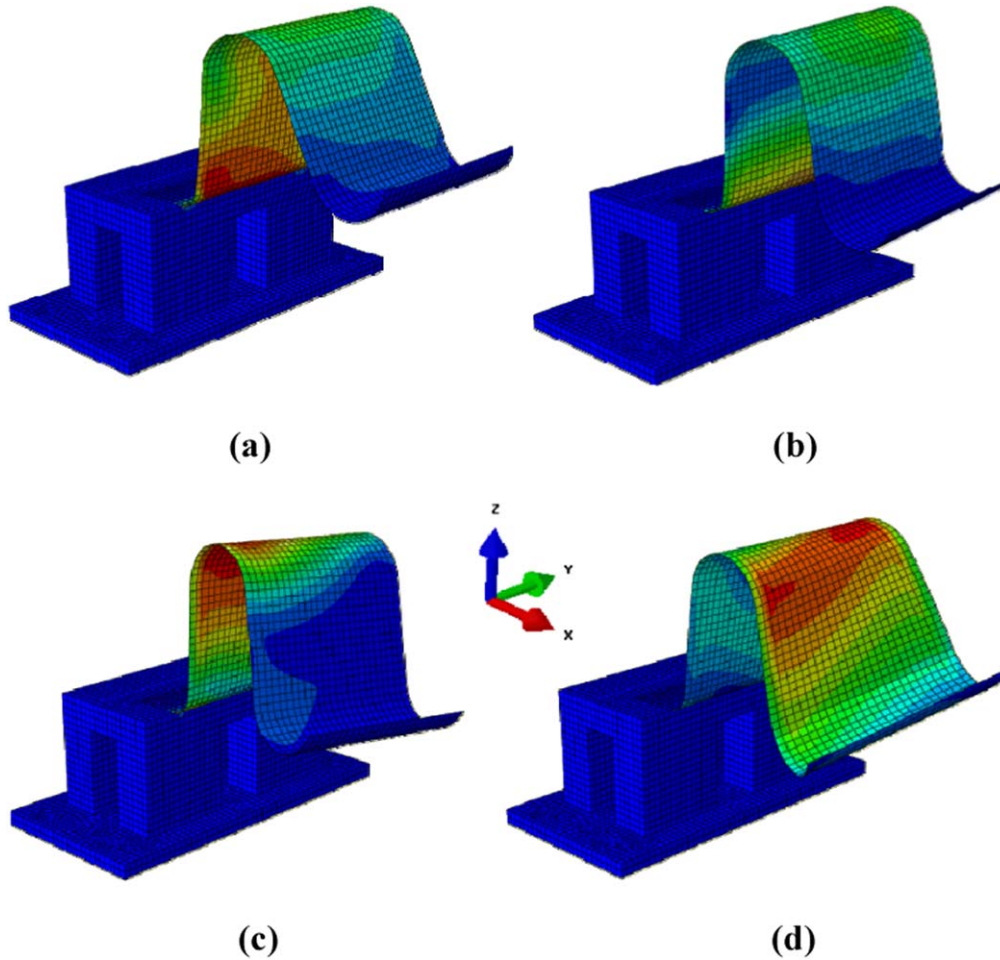


Figure 5. The first four order vibration modes of the condition 1 in packaged configuration, (a) the first mode, (b) the second mode, (c) the third mode, (d) the fourth mode.

Table 3. Material parameters of the unidirectional carbon fiber reinforced epoxy-based SMPC.

Temperature (°C)	E_1 (MPa)	E_2 (MPa)	ν_{12}	G_{12} (MPa)	G_{13} (MPa)	G_{23} (MPa)
25	30 000	2800	0.35	1500	1500	1000
100	2000	18	0.45	1.5	1.5	1

E_1 , E_2 : the Young's moduli in the X_1 , X_2 directions, ν_{12} : the major Poisson's ratio, G_{12} , G_{13} , G_{23} : the transverse shear moduli in planes X_1 - X_2 , X_1 - X_3 , X_2 - X_3 , respectively. X_1 , X_2 , X_3 : the Cartesian axes x , y and z , X_1 direction being parallel to the fibers.

Table 4. The first four order natural frequencies of different structures in packaged configuration.

No. of condition	Natural frequencies (Hz)			
	1st	2nd	3rd	4th
1	35.2	76.8	87.4	247.8
2	35.2	76.6	87.7	287
3	35.5	77.6	86.8	219.3
4	28.9	45.3	65.2	203.1
5	53.8	109.2	113.5	303.2
6	25.9	47.2	57.2	192.4
7	19.2	37.1	42.8	157.9

partial internal stress of substrate and make it better shaped. After another 20 min reheating, the oven was switched off, and the whole set was cooled down to room temperature inside the oven. Eventually, the folded sunlight-stimulated substrate was taken out from the mold. As presented in figure 7, the mold was more curved than the folded substrate because the substrate would have a slight elastic recovery once demoulded. We have taken that into account and ensured the final shape has two 10 mm radius semicircles and one 10 mm radius quadrant.

The base was milled from an aluminium alloy block and hollowed out to reduce weight on the basis of meeting

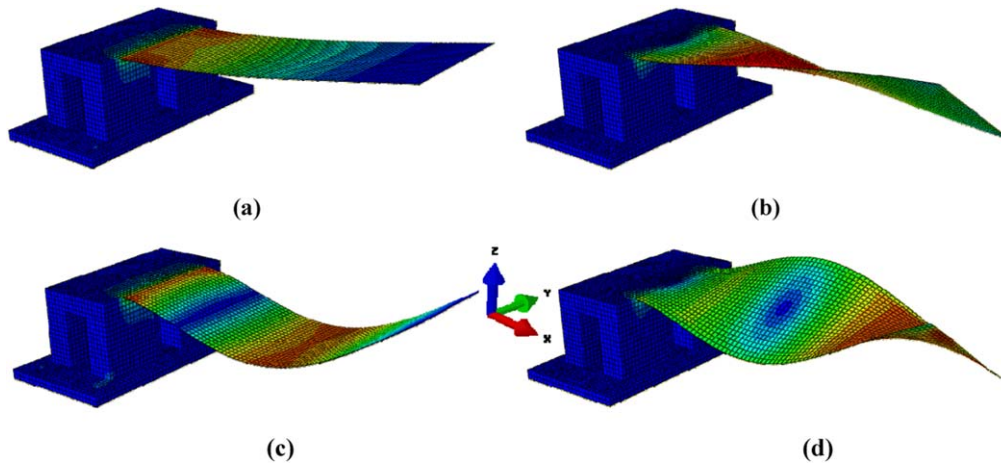


Figure 6. The first four order vibration modes of the condition 1 in deployed configuration, (a) the first mode, (b) the second mode, (c) the third mode, (d) the fourth mode.

Table 5. The first four orders of natural frequency of different structures in deployed configuration.

No. of condition	Natural frequencies (Hz)			
	1st	2nd	3rd	4th
1	2.07	13.61	32.54	36.69
2	1.75	12.22	28.88	39.54
3	2.49	15.27	28.60	44.60
4	1.46	9.89	26.95	28.54
5	3.34	20.73	39.54	52.75
6	1.38	9.42	25.82	27.96
7	0.94	6.63	18.99	23.46

strength requirement. The cap was an aluminium alloy plate with four holes at the corner. Each edge of the base and cap in contact with the substrate was chamfered to avoid shearing the substrate during vibration. The substrate was placed between the base and the cap, and both interfaces were brushed with silicon rubber to enhance contact and increase damping. Moreover, the base, substrate, and cap were screwed together by titanium hexagonal socket cylindrical head screws in flight article while stainless steel screws in test article. The thermistor was stuck to the opposite surface of base under the substrate by using silicon rubber, and its conductors were stuck to the frame of the base. Multi-layer insulation was covered around the base in flight article. The physical structure is presented in figure 8. The envelope size of the structure in packaged configuration is 100 mm × 100 mm × 87 mm, while 188 mm × 100 mm × 43 mm in deployed configuration, and the total mass is about 0.3 kg.

4. Ground experiments

Two identical Mission SMS-I structures were prepared, test article for ground-based verification, and flight article for ground-based acceptance experiments and spaceflight experiment. The test article went through vibrations, shock experiment, vacuum thermal cycling, and on-ground deployment. The

flight article underwent vibrations, vacuum thermal cycling, and on-orbital deployment.

4.1. Experimental setups

Swept sine and random vibration experiments were performed on an electro-dynamic vibration testing system. Since the acceleration sensor's weight was close to the substrate's, a foil gage was chosen and stuck to the top of the substrate (shown in figure 9(a)). The structure was tested in three mutually perpendicular directions, X, Y, Z as shown in Abaqus simulation. The required-level experimental conditions are shown in figures 9(b) and (c). Characteristic swept sine vibration experiments with experimental condition of 5–1000 Hz, 0.5 g, 1 oct min⁻¹, were carried out before and after the required-level experiments to assess the influence of vibration.

Shock experiment was carried out on a drop-hammer shock testing machine in the same directions as above. The test condition is shown in figure 10(b), where the red lines are the upper and bottom limitations, the black line is the actual control plot recorded by the acceleration sensor fixed on the testing platform. Due to the limitation of the foil gage, no data on the substrate was collected. The test was verified by checking the geometry, morphology of the substrate after shocking.

The vacuum thermal cycling experiment was conducted in a ground-based thermal vacuum chamber with experimental conditions of 6.5 cycles, vacuum pressure $\leq 6.65 \times 10^{-3}$ Pa, temperature range -145°C – 150°C , heating and cooling rate $\geq 1^\circ\text{C min}^{-1}$. Four substrates circled in red in figure 11 were tested. The controlled thermocouple of the system was fixed on one of substrates. The mechanical and shape memory properties of substrates were tested after the cycling.

The schematic of the ground-based deployment experiment is demonstrated in figure 12. A tungsten halogen lamp with a rated voltage of 220 V and power of 300 W was placed at a distance of 0.45 m to the substrate to simulate sunlight irradiation. A camera and a thermal infrared imager were

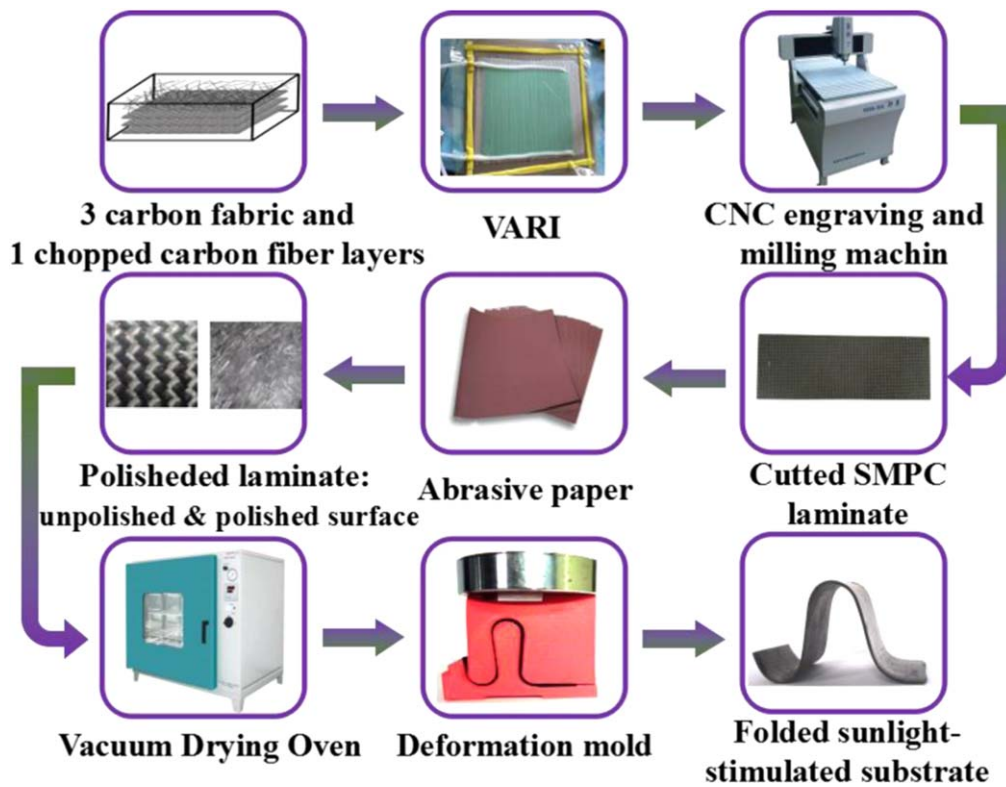


Figure 7. Schematic of the Sunlight-stimulated substrate manufacture process.

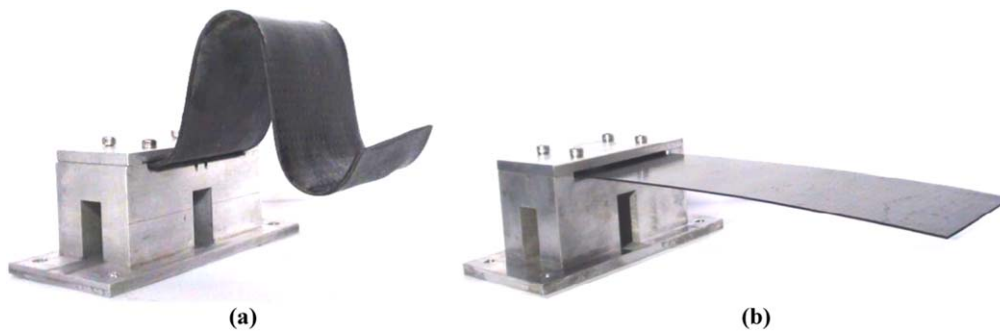


Figure 8. The configurations of Mission SMS-I, (a) packaged configuration, (b) deployed configuration.

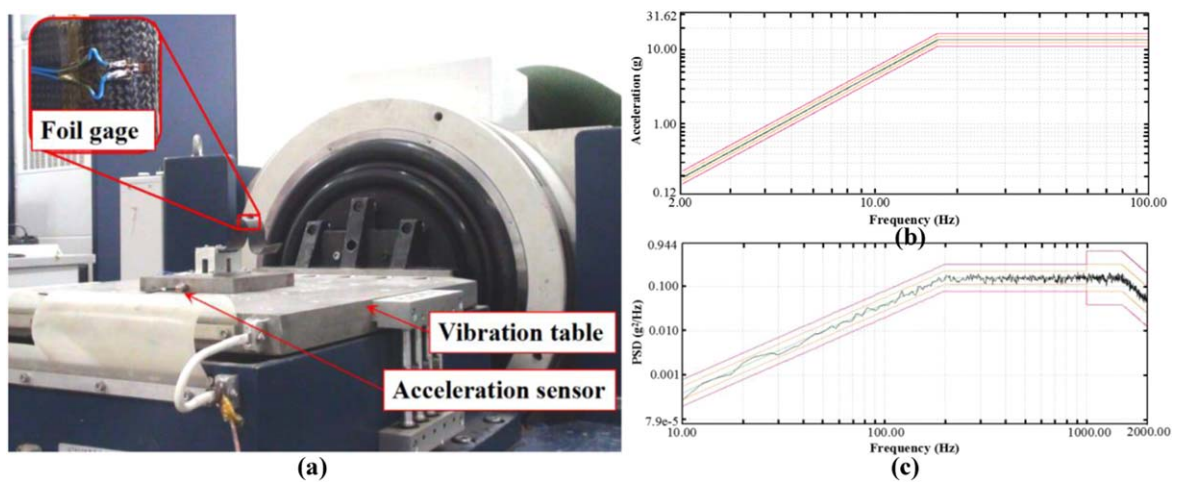


Figure 9. Vibration experiment, (a) setup in Y direction, (b) control plot for swept sine vibration, (c) control plot for random vibration.

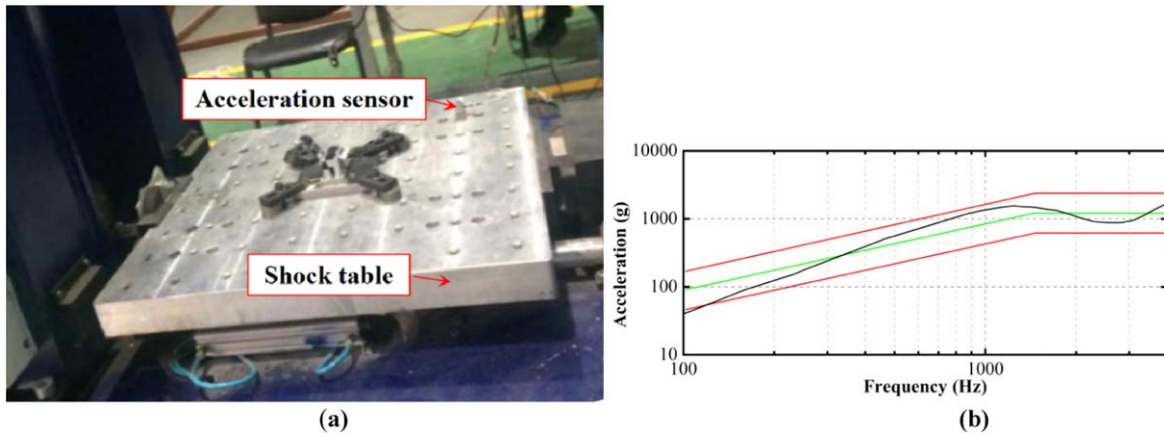


Figure 10. Shock experiment, (a) setup in X direction, (b) shock response spectrum.

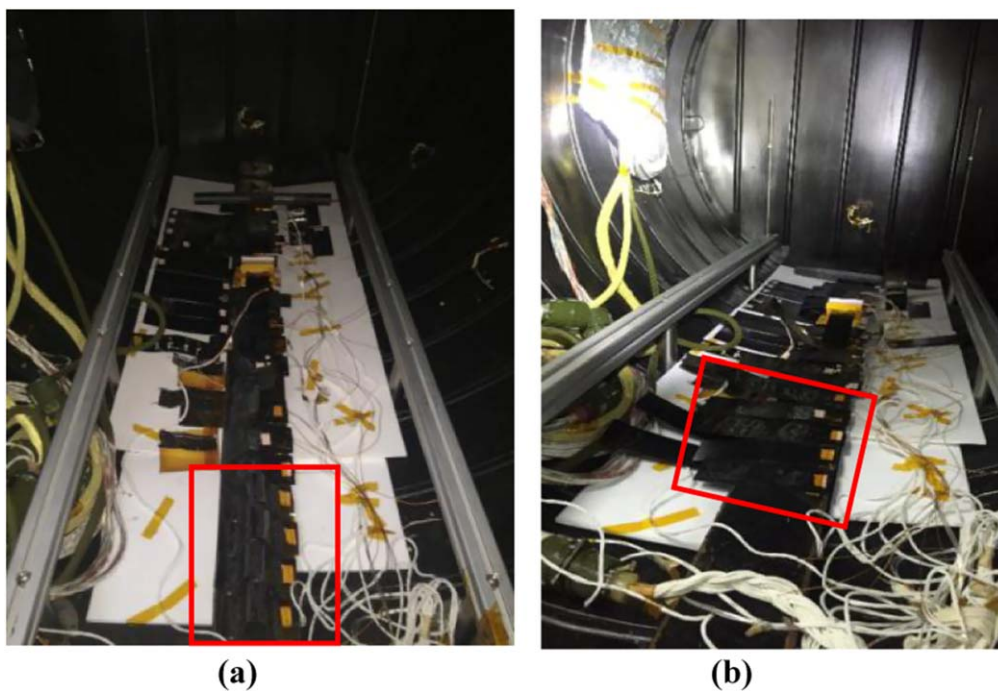


Figure 11. The images of substrates in thermal vacuum chamber (a) before thermal cycling, (b) after thermal cycling.

arranged to record the trajectory and the thermal distribution of the substrate during the deployment process.

4.2. Results and discussions

The foil gage responses at the required-level swept sine and random vibrations are presented in figure 13. Figure 13(a) shows that although the shape of the curve varies in different directions, the frequencies corresponding to the peaks of each curve are approximately the same. The resonance frequencies in X direction are 35.03 and 68.03 Hz, while 36.29, 71.45, 91.08 Hz in Y direction, and 36.13, 73.93 Hz in Z direction. The first three orders of natural frequency were calculated by using the average value of the close resonance frequency in different directions. Result is shown in table 6, showing good consistency with the result obtained by FEM simulation. The relative errors are $\sim 1.8\%$, $\sim 7.9\%$ and $\sim 4.1\%$ respectively.

This is acceptable and inevitable due to the simplification of FEM model and experimental error. Figure 13(b) presents results of the random vibration in the time domain. The maximum strain in X direction is $\sim 359 \mu\epsilon$, higher than the $\sim 91 \mu\epsilon$ and $\sim 165 \mu\epsilon$ in Y and Z directions. But they are much lower than those in the swept sine vibration, where the maximum strains are $\sim 1825 \mu\epsilon$ (X), $\sim 276 \mu\epsilon$ (Y), and $\sim 697 \mu\epsilon$ (Z). The results of the characteristic swept sine vibrations before and after the required-level swept sine/random vibrations were compared; the strain-frequency curves, including curve shape, peak location, and value, were almost the same, which meant there was no difference of the structure before and after the vibration. No damage was observed after all vibrations.

Upon impact, the structure had a rigid motion with the shock table, no noticeable jitter of the substrate was observed. After shocking, the geometry and surface of the substrate

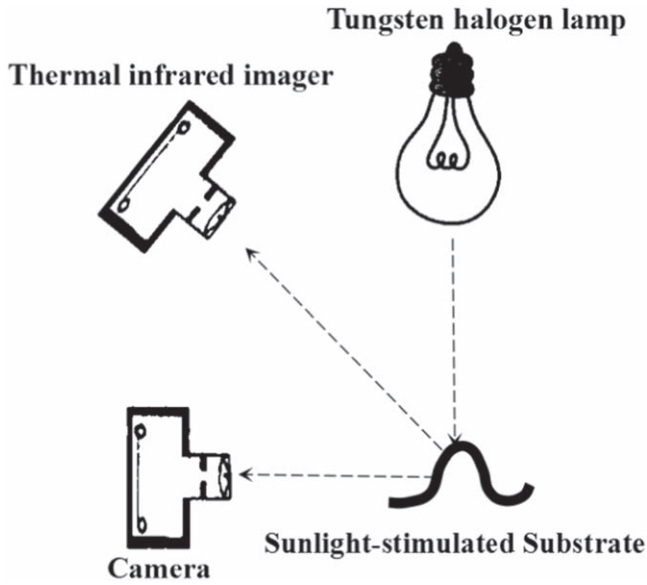


Figure 12. Schematic of sunlight-stimulated substrate's ground-based deployment experiment setup.

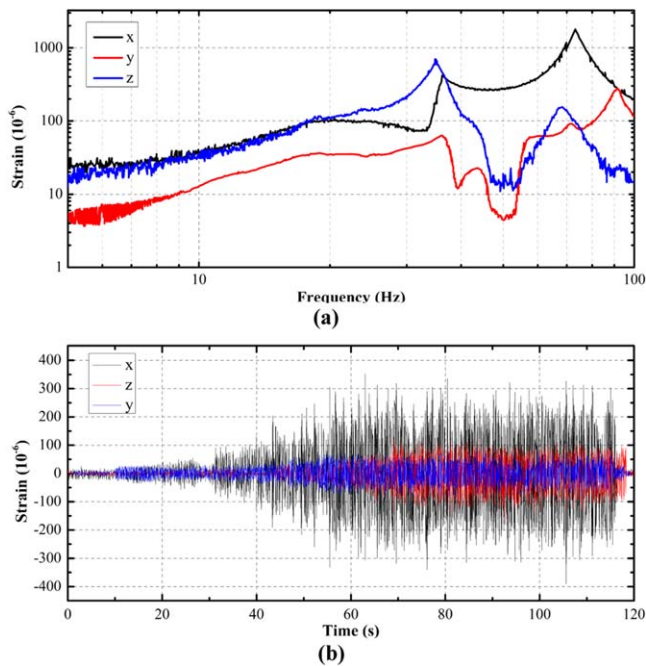


Figure 13. Foil gage responses in X, Y, Z directions, (a) swept sine vibration experiments, (b) random vibration experiments.

Table 6. Comparison of experimental and simulation results of natural frequency.

The order of mode	Experimental results (Hz)	Simulation results (Hz)
1st	35.81	35.17
2nd	71.14	76.78
3rd	91.08	87.38

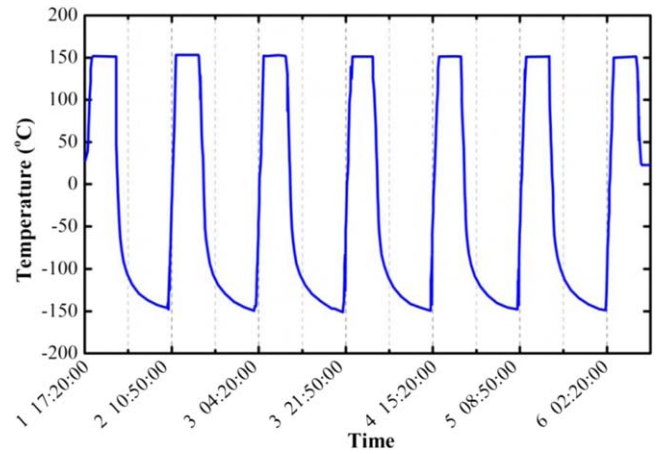


Figure 14. The temperature-time curve at control point.

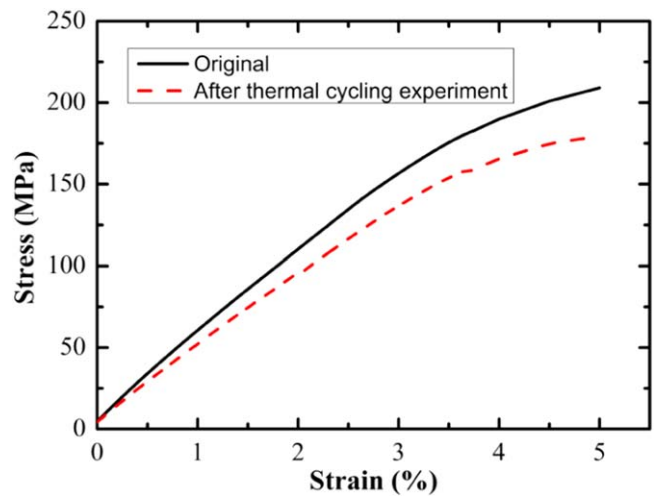


Figure 15. Three-point bending results of specimens before and after thermal cycling experiment.

were checked, and no deformation or crack was detected. The thermistor adhered well to the base surface and can still monitor the temperature changes. Although there was no direct shock response of the substrate, the observation results still indicated that Mission SMS-I had an excellent shock resistance, no electrical or mechanical damage occurred during testing.

The temperature-time curve of the controlled thermocouple is shown in figure 14, the shape repeats well in every cycle. All substrates recovered to the flat configuration after the first cycle, because the matrix's T_g of 85.4 °C was within the temperature range of the thermal cycling. A comparison of the three-point bending tests before and after thermal cycling was conducted at room temperature. Figure 15 illustrates that the flexural modulus of the original specimen which has neither be deformed nor heated is 5.63 GPa, while 4.80 GPa of the specimen after experiencing vacuum thermal cycling. The result of the thermally cycled specimen is close to the result of the Series B in section 2.2, indicating that mechanical properties have barely been reduced by thermal

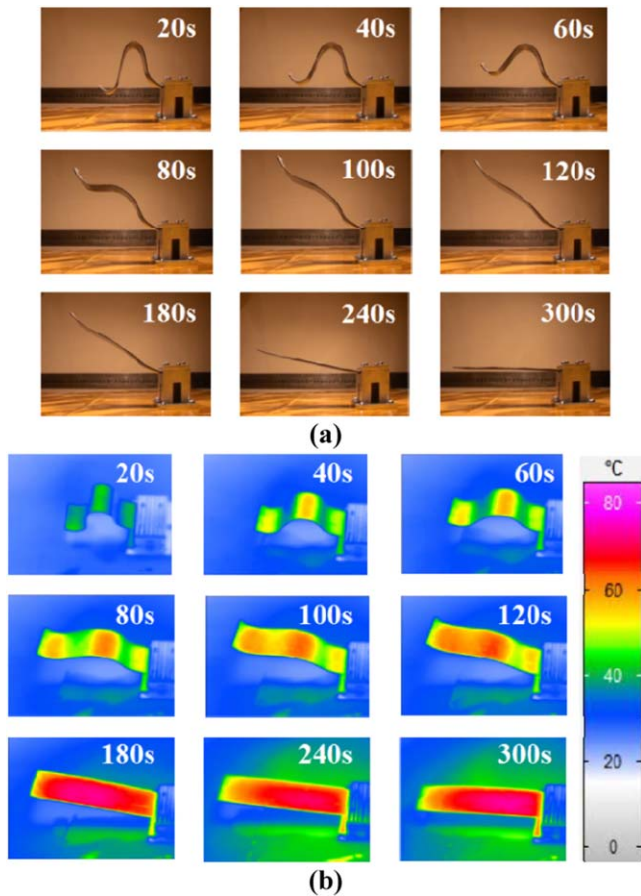


Figure 16. The deployment of sunlight-stimulated substrate at ground-based deployment experiment, (a) camera images, (b) thermal infrared imager images.

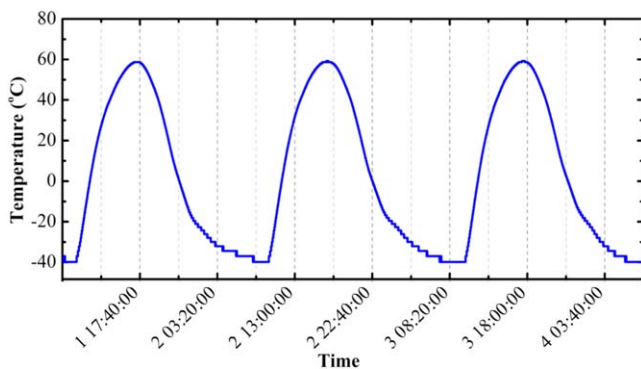


Figure 17. Typical temperature cycle collected by the thermistor.

cycling, but by the micro-buckling of fabric as explained above. In addition, one of the substrates was bent into the ‘U’ shape with a radius of 10 mm and recovered to flat upon reheating. These results indicate that the temperature variation does not affect the shape memory property of the substrate.

The substrate exhibited a ‘Ω’ configuration at the beginning, resulting in a shorter distance from the top of the substrate to the lamp than from the valley to lamp. Figure 16(b) demonstrates that the maximum local temperature of the intermediate curved portion reached $\sim 54^\circ\text{C}$ after 20 s of continuously irradiation, while the unirradiated area

(the surfaces perpendicular to light) was $\sim 17^\circ\text{C}$. Therefore, the intermediate portion deployed firstly. In figure 16, the intersection angle of the two straight lines in the middle of the substrate increases from $\sim 0^\circ$ to $\sim 180^\circ$. The angle differences between adjacent images in figure 16(a) are 12.2° , 19.2° , 57.87° , 32.15° , 16.03° , 6.25° , 9.00° , and 0° in sequence, presenting a slow–fast–slow changing tendency. During the initial preheating process, the matrix of the SMPC gradually transferred to rubbery phase and started to deploy; the deployment speed increased with the temperature increased. But as the stored energy was released with recovery, the deployment speed slowed down and went to zero eventually. The portion of the substrate near the unirradiated base was the last to recover since the heat there was partially conducted to the base. The total recovery time was ~ 300 s with the recovery ratio $\sim 100\%$.

5. Orbital experiment

The launch of the experimental satellite took place in 2016. The Mission SMS-I structure was installed on the west deck of the satellite. There were only two telemetries during the orbital experiment: images captured by the satellite camera, and the temperature measured by thermistor located inside the aluminum base. The image was adopted to evaluate the performance of the substrate, including recovery ratio and surface morphology. The thermistor recorded the temperature during spaceflight, hinting the exposure and shadow time of the substrate to the Sun.

Figure 17 exhibits three typical temperature cycles collected by the thermistor. The cycle repeated well with a temperature range from -40°C to 60°C . One complete cycle lasted about 24 h, the duration of temperature above 0°C was ~ 12 h, and ~ 4 h above 50°C . Whereas, the temperature range of the substrate should be larger than telemetry data since the thermistor located inside the base, which was covered by insulation multilayer. Considering the T_g of the matrix to be 85.4°C , we inferred that the maximum temperature of the substrate should be at least 20°C higher than the telemetry data.

There were three spaceflight observations, first on 13 d after launch, followed by the second 3 d later, and the third 8 months later. Images shot on the first two observations were visually identical since the interval was short. Only the first orbital images are presented here. The outline of the substrate was drawn with red dashed lines. The side view in figure 18(a) indicates that the substrate has recovered to the flat configuration with a recovery ratio of $\sim 100\%$. No crack is observed on the upper surface in figure 18(b). The deployment process cannot be recorded due to the limitation of operation, thus we present an animation in the supporting information is available online at stacks.iop.org/SMS/28/075023/mmedia. It was acceptable that the substrate softened under sunlight. The only requirement for Mission SMS-I in deployed configuration was that the first order of natural frequency must be above 2 Hz, which has been stated in section 3.2. Actually, the satellite was large, whose weight

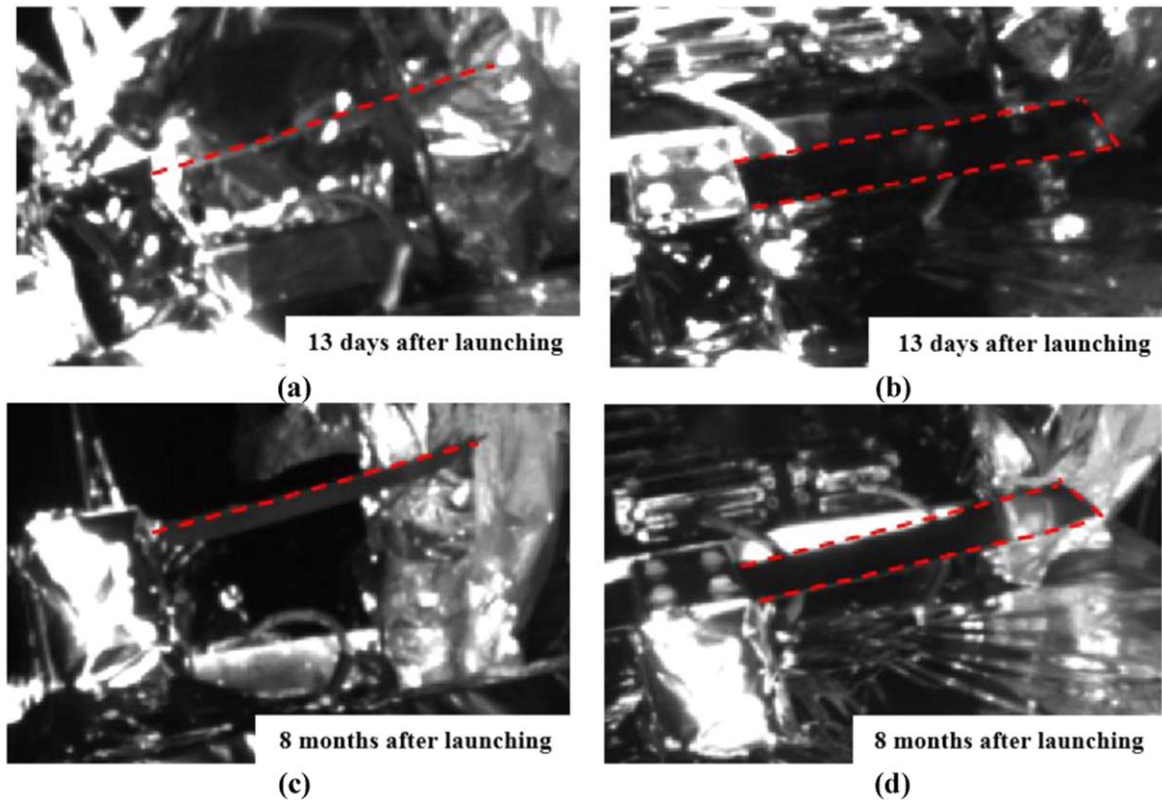


Figure 18. Orbital images, (a) side view of the first observation, (b) oblique view of the first observation, (c) side view of the third observation, (d) oblique view of the third observation.

was four orders of magnitude higher than Mission SMS-I, and its slow attitude transformation could hardly affect the small substrate. Moreover, the flexural modulus of the substrate was higher than that of the epoxy at 120 °C, which was ~250 MPa even if it had been deformed once. Eight months later, the substrate still performed a straightly flat configuration without visible crack (figures 18(c) and (d)), proving the SMPC had a good long-term anti-irradiation capability.

6. Conclusion

Mission SMS-I, a sunlight-stimulated substrate based on carbon fabric reinforced SMPC, has gone through material preparation, structure design, assembly, ground experiments, and orbital verification. Material properties of SMP and SPMC have been characterized by DMA and three-point bending experiments. The T_g of the matrix is 85.4 °C. The flexural modulus and strength of the SMPC specimens which have been deformed once are slightly lower than the original ones, but still higher than the SMP. The structure design has drawn on the experience of conventional solar arrays, and aided by FEM simulation, the first order of natural frequency is 35.17 Hz in packaged configuration and 2.07 Hz in the deployed configuration. Results from ground experiments indicate the substrate can withstand required mechanical and thermal environments and could be stimulated by light irradiation. The successful orbital experiment shows that the substrate could deploy without satellite electric energy, and

SMPC is a suitable material for components exposed to space environment directly. It is the world's first SMPC spaceflight experiment in geostationary orbit, and China's pioneering SMPC spaceflight experiment.

7. Perspectives

Unpredictable spaceflight anomalies generally involve failures related to spacecrafts' appendages (i.e. solar arrays, antennas, booms, etc) deployment, such as malfunctions of Magellan satellite's solar array latch and Arabsat satellite's solar array deployment [41]. The sunlight-stimulated SMPC-based components might be an effort to eliminate anomalies by replacing conventional kinematic pairs, such as hinges for solar arrays or antennas [35], hooks or bolts for different release devices (i.e. Marmon band release device [42], explosive bolt, frangibolt [43], etc). Upon release/deployment, the spacecraft can adjust its attitude to expose the SMPC-based component to the Sun for deployment. Compared to the conventional release or deployment system, the absence of complex mechanical devices of the Sunlight-stimulated system vanishes the possible problems of large impact of pyrotechnics, cold welding, clamping stagnation, and abnormal circuit, improving the operation reliability.

The sunlight-stimulated SMPC is extremely suitable for appendages which are required to operate immediately once in orbit. It has a high potential to be used in CubeSats or SmallSats, whose technical challenges may include the

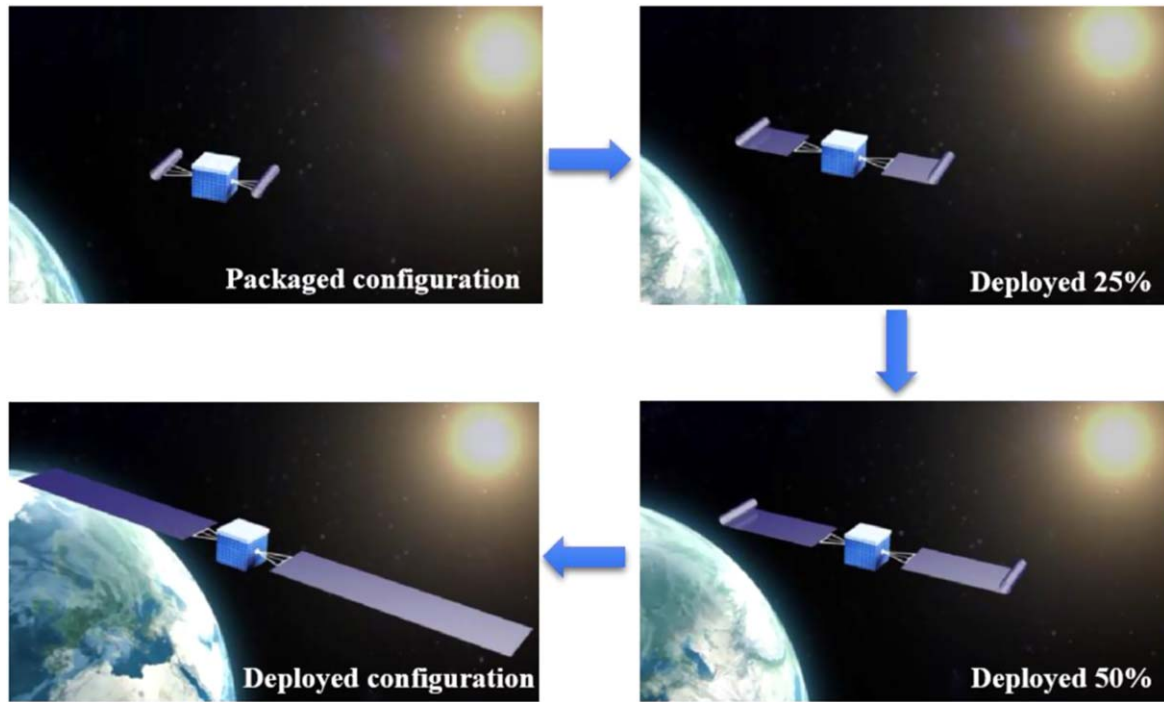


Figure 19. Deployment schematic of the future sunlight-stimulated rollable solar array.

limited surface area on the external walls for solar cell assembly and the lack of sufficient power storage to orbital tasks. The sunlight-stimulated substrate with various folding patterns (i.e. the accordion-fashion in figure 3, the rollable-fashion in figure 19) could be a reasonable alternative for future solar arrays of miniaturized satellites because of its small volume, lightweight, and the Sunlight-stimulated deployment mechanism. Its relatively small deployed-size is not too large to be stiff enough. Efforts are being made to develop new sunlight-stimulated SMPC with higher stiffness under the Sunlight.

Along with the Sunlight-stimulated SMPC development, we have been studied the SMPC with higher T_g (i.e. cyanate-based SMPs with T_g range of 156.9 °C–256.9 °C [18], Polyimide-based SMPs with T_g range of 321 °C–323 °C [21]) aimed for active deployment. Its T_g is higher than the temperature that can be reached by sunlight irradiation. Though external heaters are required to stimulate the SMPC, the material hardens again after cutting off the electrical supply, offering design possibilities for large deployable structures, such as a rollable solar array in ROSA dimension [10], but without mechanical assistance to maintain the deployed configuration.

The SMPC could be designed to various components since they are deformable, portable. Besides light weight and deformable advantages, it also reduces the mechanical complexity of the components, increases operational reliability and saves energy for the spacecraft. We have seen this material, if incorporated with origami-inspired designs, would enable the passive/active deployment of large and multi-functional deployable structures.

Acknowledgments

The authors would like to thank all members in Smart Material and Structure group in Harbin Institute of Technology for their contributions. This work is supported by the National Natural Science Foundation of China: Grant No. 11672086, 11772109 and 11632005.

ORCID iDs

Yanju Liu  <https://orcid.org/0000-0001-8269-1594>

Jinsong Leng  <https://orcid.org/0000-0001-7249-9101>

References

- [1] Baghdasarian V G 1998 Hybrid solar panel array *US Patent Specification* 5785280
- [2] Brandhorst H W and Rodiek J A 2008 Space solar array reliability: a study and recommendations *Acta Astronaut.* **63** 1233–8
- [3] Ercol C J, Jenkins J, Dakermanji G, Santo A G and Mason L S 2000 Prototype solar panel development and testing for a Mercury orbiter spacecraft *235th Intersociety Energy Conversion Engineering Conf. and Exhibit (Las Vegas, NV, USA, July)* pp 449–59
- [4] Xilun D, Xin L, Kun X, Qiaolong Y and Hailing P 2012 Study on the behaviour of solar array deployment with root hinge drive assembly *Chin. J. Aeronaut.* **25** 276–84
- [5] Ding X and Li X 2014 Design and test analysis of a solar array root hinge drive assembly *Chin. J. Mech. Eng.* **27** 909–18
- [6] Blanc A, Chassoulier D, Champandard F and Francois X 2013 Solar array root hinge based on shape memory alloy (SMA) actuator *15th European Space Mechanisms & Tribology*

- Symp.-ESMATS (Noordwijk, Netherlands, September)* pp 25–7
- [7] Maly J R, Pendleton S C, Salmanoff J, Blount G J and Mathews K 1999 Hubble space telescope solar array damper *Smart Structures and Materials Proc. SPIE 3672, Smart Structures and Materials 1999: Passive Damping and Isolation (Newport Beach, CA, US, June)* pp 186–98
- [8] Johnston J D and Thornton E A 2000 Thermally induced dynamics of satellite solar panels *J. Spacecr. Rockets* **37** 604–13
- [9] Hoffman D J, Kerslake T W, Hepp A F, Jacobs M K and Ponnusamy D 2000 Thin-film photovoltaic solar array parametric assessment [space power] *35th Intersociety Energy Conversion Engineering Conf. and Exhibit (Las Vegas, NV, USA, July)* pp 670–80
- [10] Hoang B, White S, Spence B and Kiefer S 2016 Commercialization of Deployable Space Systems' roll-out solar array (ROSA) technology for Space Systems Loral (SSL) solar arrays 2016 *IEEE Aerospace Conf. (March)* (<https://doi.org/10.1109/AERO.2016.7500723>)
- [11] Medford A J, Lilliedal M R, Jørgensen M, Aarø D, Pakalski H, Fyenbo J and Krebs F C 2010 Grid-connected polymer solar panels: initial considerations of cost, lifetime, and practicality *Opt. Express* **18** A272–85
- [12] Ferris M and Haslehurst A 2014 The use, evolution and lessons learnt of deployable static solar array mechanisms *The 42nd Aerospace Mechanism Symp.* pp 421–34
- [13] Gibb J and Billets S 2010 A case study: integrating triple-junction solar cells into flat-folding flexible solar array panels *35th IEEE Photovoltaic Specialists Conf. (Honolulu, HI, USA, June)* pp 000731–5
- [14] Fang H, Lou M and Hah J 2006 Deployment study of a self-rigidizable inflatable boom *J. Spacecr. Rockets* **43** 25–30
- [15] Huang J 2001 The development of inflatable array antennas *IEEE Antennas Propag. Mag.* **43** 44–50
- [16] Rauschenbach H S 2012 *Solar Cell Array Design Handbook: The Principles and Technology of Photovoltaic Energy Conversion* (New York: Van Nostrand Reinhold Company) p 337
- [17] Leng J, Lan X, Liu Y and Du S 2011 Shape-memory polymers and their composites: stimulus methods and applications *Prog. Mater. Sci.* **56** 1077–135
- [18] Xie F, Huang L, Liu Y and Leng J 2012 Modified shape memory cyanate polymers with a wide range of high glass transition temperatures *Proc. SPIE* vol **8342** 834210
- [19] Behl M, Razaq M Y and Lendlein A 2010 Multifunctional shape-memory polymers *Adv. Mater.* **22** 3388–410
- [20] Song J J, Chang H H and Naguib H E 2015 Biocompatible shape memory polymer actuators with high force capabilities *Eur. Polym. J.* **67** 186–98
- [21] Xiao X, Kong D, Qiu X, Zhang W, Zhang F, Liu L, Liu Y, Zhang S, Hu Y and Leng J 2015 Shape-memory polymers with adjustable high glass transition temperatures *Macromol.* **48** 3582–9
- [22] Tobushi H, Hara H, Yamada E and Hayashi S 1996 Thermomechanical properties in a thin film of shape memory polymer of polyurethane series *Smart Mater. Struct.* **5** 483
- [23] Li F, Scarpa F, Lan X, Liu L, Liu Y and Leng J 2019 Bending shape recovery of unidirectional carbon fiber reinforced epoxy-based shape memory polymer composites *Composites A* **116** 169–79
- [24] Guo J, Wang Z, Tong L and Liang W 2016 Effects of short carbon fibres and nanoparticles on mechanical, thermal and shape memory properties of SMP hybrid nanocomposites *Composites B* **90** 152–9
- [25] Tandon G, Goecke K, Cable K and Baur J 2009 Durability assessment of styrene-and epoxy-based shape-memory polymer resins *J. Intell. Mater. Syst. Struct.* **20** 2127–43
- [26] Ratna D and Karger-Kocsis J 2008 Recent advances in shape memory polymers and composites: a review *J. Mater. Sci.* **43** 254–69
- [27] Guo J, Wang Z, Tong L, Lv H and Liang W 2015 Shape memory and thermo-mechanical properties of shape memory polymer/carbon fiber composites *Composites A* **76** 162–71
- [28] Ohki T, Ni Q-Q, Ohsako N and Iwamoto M 2004 Mechanical and shape memory behavior of composites with shape memory polymer *Composites A* **35** 1065–73
- [29] Rossiter J, Takashima K, Scarpa F, Walters P and Mukai T 2014 Shape memory polymer hexachiral auxetic structures with tunable stiffness *Smart Mater. Struct.* **23** 045007
- [30] Barrett R, Francis W, Abrahamson E, Lake M and Scherbarth M 2006 Qualification of elastic memory composite hinges for spaceflight applications *47th AIAA/ASME/ASCE/AHS/ASC Structures, Structural Dynamics, and Materials Conf. 14th AIAA/ASME/AHS Adaptive Structures 7th Conf. (Newport, Rhode Island, May)* p 2039
- [31] Sokolowski W M and Tan S C 2007 Advanced self-deployable structures for space applications *J. Spacecr. Rockets* **44** 750–4
- [32] Li F, Liu L, Lan X, Zhou X, Bian W, Liu Y and Leng J 2016 Preliminary design and analysis of a cubic deployable support structure based on shape memory polymer composite *Int. J. Smart Nano Mater.* **7** 106–18
- [33] Beavers F, Munshi N, Lake M, Maji A, Qassim K, Carpenter B and Rawal S P 2002 Design and testing of an elastic memory composite deployment hinge for spacecraft *43rd AIAA/ASME/ASCE/AHS/ASC Structures, Structural Dynamics, and Materials Conf. (Denver, Colorado, April)* p 1452
- [34] Keller P, Lake M, Francis W, Harvey J, Ruhl E, Winter J, Scherbarth M S and Murphey T W 2004 Development of a deployable boom for microsattellites using elastic memory composite material *45th AIAA/ASME/ASCE/AHS/ASC Structures, Structural Dynamics & Materials Conf. (Palm Springs, California, April)* p 1603
- [35] Liu Y, Du H, Liu L and Leng J 2014 Shape memory polymers and their composites in aerospace applications: a review *Smart Mater. Struct.* **23** 023001
- [36] Santo L, Quadrini F, Squeo E A, Dolce F, Mascetti G, Bertolotto D, Villadei W, Ganga P L and Zolesi V 2012 Behavior of shape memory epoxy foams in microgravity: experimental results of STS-134 mission *Microgravity Sci. Technol.* **24** 287–96
- [37] Santo L, Quadrini F, Ganga P L and Zolesi V 2015 Mission BION-M1: results of Ribes/Foam2 experiment on shape memory polymer foams and composites *Aerosp. Sci. Technol.* **40** 109–14
- [38] Leng J, Wu X and Liu Y 2009 Effect of a linear monomer on the thermomechanical properties of epoxy shape-memory polymer *Smart Mater. Struct.* **18** 095031
- [39] Leng J, Xie F, Wu X and Liu Y 2014 Effect of the γ -radiation on the properties of epoxy-based shape memory polymers *J. Intell. Mater. Syst. Struct.* **25** 1256–63
- [40] Tan Q, Li F, Liu L, Chu H, Liu Y and Leng J 2018 Effects of atomic oxygen on epoxy-based shape memory polymer in low earth orbit *J. Intell. Mater. Syst. Struct.* **29** 1081–7
- [41] Freeman M T 1993 Spacecraft on-orbit deployment anomalies: what can be done? *IEEE Aerosp. Electron. Syst. Mag.* **8** 3–15
- [42] Peffer A, Denoyer K, Fosness E and Sciulli D 2000 Development and transition of low-shock spacecraft release devices *2000 IEEE Aerospace Conference. Proceedings (Cat. No. 00TH8484)* vol 4 (Piscataway, NJ: IEEE) pp 277–84
- [43] Pacheco P and Savi M A 2000 Modeling and simulation of a shape memory release device for aerospace applications *Rev. Eng. Ciênc. Aplicadas* 1–16